# A numerical analysis of aluminum droplet combustion driven instabilities in solid rocket motors

Aurelien Genot, Stany Gallier, Thierry Schuller

DOI: 10.13009/EUCASS2017-64



DOI: ADD DOINUMBER HERE

# A numerical analysis of aluminum droplet combustion driven instabilities in solid rocket motors

Aurelien Genot[1,2,3†], Stany Gallier[2] and Thierry Schuller[3,4]
[1]*CNES DLA, Centre National d'Etudes Spatiales, Direction des lanceurs, 52 rue Jacques Hillairet, 75612 Paris cedex, France*
[2]*Airbus Safran Launchers, Centre de Recherche du Bouchet, 9 rue Lavoisier, 91710 Vert-le-Petit, France*
[3]*Laboratoire EM2C, CNRS, CentraleSupelec, Université Paris Saclay*
*Grande voie des vignes, 92295 Châtenay-Malabry, France*
[4]*Institut de Mécanique des Fluides de Toulouse (IMFT), Université de Toulouse, CNRS, INPT, UPS, Toulouse, France*
[†]Corresponding author: aurelien.genot@centralesupelec.fr

## Abstract

Acoustic coupling with unsteady aluminum particle combustion may lead to self-sustained instabilities with large oscillation amplitudes in a solid rocket motor. A numerical analysis of this phenomenon is carried out for instabilities and at instability limit cycles in a set of generic configurations. It is found that the synchronized combustion oscillations can be split in two different contributions to heat release disturbances driving the instability. In the combustion volume, volumetric heat release rate fluctuations result from the cumulative contribution of burning rate oscillations of each individual aluminum droplet experiencing an oscillating drag. The second contribution to heat release oscillations in the SRM corresponds to the motion of the aluminum combustion zone boundary. In the configurations explored, this contribution may reach up to about 40% of the total heat release rate oscillation in the motor and is shown to depend on the way the end life of aluminum droplets is modeled.

## 1. Introduction

Undesirable self-sustaining oscillations of pressure are observed in most solid rocket motors (SRM).[1] These unsteady phenomena may lead to thrust oscillations or high vibration levels which are transmitted to the launcher.[1] They usually result from flow instabilities, which, by phenomena of resonance with the acoustics of the motor, reach limit cycles before possibly disappearing when resonance conditions are no longer fulfilled. There are various types of acoustic triggered flow instabilities, in particular those linked to hydrodynamics and those associated with combustion.

In small lab scale motors, high frequency combustion instabilities due to propellant combustion-acoustic coupling are often observed because the combustion propellant response amplifies flow perturbations at these acoustic frequencies.[2,3] For larger motors, pressure oscillations are often due to vortex shedding-acoustic coupling and the solid propellant combustion contribution to these instabilities remains weak.[4,5] There is however another category of combustion instabilities where the direct propellant combustion response to acoustic waves is not significant, but it is the unsteady combustion response of aluminum droplets released by the propellant that drives the thermo-acoustic coupling. These instabilities have a much lower frequency and may appear in large rocket motors.

These combustion instabilities have so far been rarely studied.[6–8] In 1971, Beckstead and Culick[9] found inconsistent results in T-burner experiments with the state-of-the art of combustion instability theory in SRM. Dupays and Vuillot[7,10] later demonstrated that the unsteady mass release from a cloud of vaporizing droplets could amplify acoustic waves. Brooks *et al.*[6] studied effects of aluminum distributed combustion in a Rijke burner and found that aluminum droplet combustion can drive a thermo-acoustic instability. However, the results from this lab scale experiment is not directly extendable to a SRM because combustion is distributed all along the acoustic mode and the temperature gradient is perpendicular to the acoustic modes in the SRM whereas it is parallel in a Rijke tube burner. Also, thermo-acoustic instabilities associated to aluminum droplet combustion are suspected in the data analyzed of the SENTRY ballistic missile defense motor.[11] Finally, Gallier and Godfroy[8] proved numerically the existence of aluminum combustion driven instabilities in a generic SRM for simulations carried out without turbulence and where large vortical structures and the propellant response to sound waves can be neglected.

The source of these latter thermo-acoustic instabilities originates from the coupling between flow perturbations and the combustion response of the aluminum droplets in the SRM.[1] It is shown in this article that in such case the

DOI: 10.13009/EUCASS2017-64



distribution of heat release rate fluctuations in the motor results both from the unsteady response of aluminum droplets in a fixed combustion volume and from the oscillation of the boundary of the combustion volume. It also demonstrated that this second contribution to the Rayleigh source term highly depends on the droplet combustion model used in the simulations.

The article is organized as follows. The aluminum combustion model used for the simulations is presented in section 2. This is followed by the numerical setup, the flow solver and the boundary conditions in section 3. Numerical results and analysis of self-sustained combustion instabilities at limit cycle are examined in section 4. These data are used to identify the different contributions to the Rayleigh source term driving the thermo-acoustic instability. A parametric analysis is finally conducted in section 5 to determine the sensitivity of these contributions to the combustion model parameters.

## 2. Aluminum droplet combustion

Aluminum droplets are surrounded by the propellant combustion products featuring oxidizing and inert gases. The main oxidizing gases are $H_2O$, $CO_2$ and HCl. Water vapor and carbon dioxide are present in large quantities in a SRM. As illustrated in Figure 1, the combustion of a solid aluminum particle is the result of a series of complex multi-physics elementary process.[12] The aluminum droplet first vaporizes, it then reacts in the gaseous phase, and finally, some gaseous products condense to form alumina $Al_2O_3$(l) in a liquid phase. Some alumina condensates at the surface of the aluminum particle, thus forming a two-constituant aluminum/alumina droplet. The droplet also loses its sphericity due to the surface tension between the aluminum and the alumina condensate. An alumina lobe progressively forms. The gas exchange surface through this new particle is in turn also modified. The alumina present in the aluminum droplet could be due to a diffusion phenomenon of the gaseous products towards the droplet, followed by a condensation on the droplet surface, or a coalescence between droplets of alumina and the aluminum droplet. Many of these process remain unclear and are still the topic of numerous investigations.[6,12–14] Numerical simulations of the multi-phase reacting flow in a SRM are thus generally based on heuristic combustion models of aluminum particle.

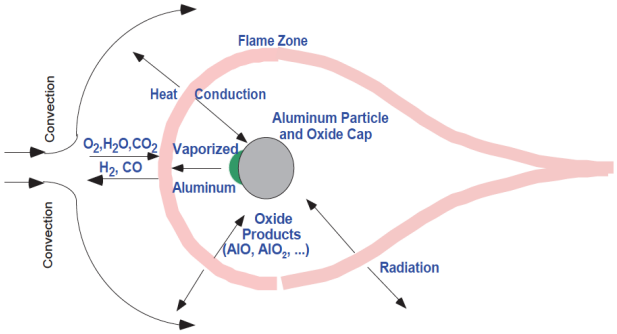


Figure 1: Sketch of aluminum droplet combustion.[12]

The alumina lobe and non-sphericity of the fuel particles are not taken into account in the modeling approach used in this work. However, it is known that the alumina residue after combustion of the metallic aluminum particle is an important feature that needs to be modeled to reproduce the acoustic losses of the motor.[1,15] The alumina residue is here considered to be a spherical residue of diameter $D_{res}$ and the aluminum combustion ceases when the diameter of the spherical aluminum droplet drops below this critical threshold.

It has been shown[16] that the flame radius $r_f$ of an aluminum particle burning in air is about twice the particle radius $r_p$:

$$r_f \simeq 2r_p \tag{1}$$

The same relation is assumed to hold here. According to Borghi and Champion,[17] if $N_p^{1/3} r_f < 0.41$, where $N_p$ is the number of fuel droplets per unit volume, the probability to get droplet group combustion, *i.e.* flames surrounding two or more droplets remains weak. When $N_p^{1/3} r_f \ll 1$ remains small, each droplet burns individually. For a mass fraction of 18% of aluminum in the solid propellant that is uniformly distributed over the combustion volume occupied by the droplets, one finds :

$$N_p^{1/3} r_f \simeq 0.1 \tag{2}$$

The same type of result was also found by post-processing the numerical data. These tests validate the hypothesis of combustion of isolated droplets in the configurations envisaged.

DOI: 10.13009/EUCASS2017-64



Simulations are carried out with an isolated droplet combustion model which is an adaptation of the $D^2$-law[18–21] to aluminum particle combustion in SRMs :

$$\frac{dD^2}{dt} = -\frac{4\dot{m}}{\pi D \rho_{Al}} = -\frac{4\mu \ln(1+B)\mathrm{Sh}}{\rho_{Al}\mathrm{Sc}} \tag{3}$$

where $D = 2r_p$ is the particle diameter, $\rho_{Al}$ is the aluminum density and $\dot{m}$ is the mass burning rate of the particle, $\mu$ is the burnt propellant gas dynamic viscosity, Sc is the Schmidt number, Sh denotes the Sherwood number and B stands for the Spalding number, which reflects effects of combustion on mass diffusion and is determined by the mass fraction of the oxidizing species. In the model used in the simulations, the Spalding number is defined as :

$$B = \frac{C_{P,g}\,(T_\infty - T_S) + \Delta h_r}{L_v} \tag{4}$$

where $L_v$ is the latent heat of vaporization of aluminum, $C_{P,g}$ is the heat capacity at constant pressure from the propellant burnt gases, $T_S$ stands for the aluminum droplet surface temperature, which is also assumed to be uniform and $T_\infty$ denotes the burnt gas temperature far from the particle. The reaction enthalpy $\Delta h_r$ is the mean enthalpy of all combustion reactions, which is known only approximately.

The Sherwood number Sh appearing in Eq. (3) determines effects of flow convection on the burning rate of the fuel particle and is given by the Ranz-Marshall correlation:[22]

$$\mathrm{Sh} = 2 + 0.6\mathrm{Re}_p^{1/2}\mathrm{Sc}^{1/3} \tag{5}$$

where the particle Reynolds number $\mathrm{Re}_p$ is calculated with a velocity $\delta\mathbf{u}_p$ corresponding to the difference between the particle velocity $\mathbf{u}_p$ and the gas velocity $\mathbf{u}$:

$$\mathrm{Re}_p = \frac{\rho_g|\mathbf{u}_p - \mathbf{u}|D}{\mu} = \frac{\rho_g|\delta\mathbf{u}_p|D}{\mu} \tag{6}$$

In this expression, $\rho_g$ denotes the propellant burnt gas density.

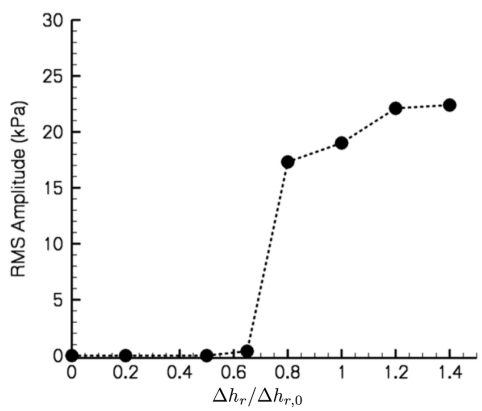


Figure 2: Enthalpy reaction effect on the root-mean-square values of pressure fluctuations of numerical simulations in a generic SRM.[8]

For the simulations presented in the next section, the value of the reaction enthalpy of the aluminum-oxygen reaction is fixed to $\Delta h_r = 9.53$ MJ/kg.[7,8] Thermodynamic calculations for typical industrial solid propellant compositions yield values between $\Delta h_r = 10$ and 20 MJ/kg.[23] The value $\Delta h_{r,0} = 9.53$ MJ/kg corresponds thus to a minimum and serves as a reference. Gallier *et al.*[8] found in their simulations that increasing the enthalpy reaction value modifies the thermo-acoustic stability of the motor. In the case explored in Figure 2, the motor is thermo-acoustic stable below the threshold $\Delta h_r/\Delta h_{r,0} \leq 0.6$ and then becomes unstable for larger reaction enthalpy values. In the unstable cases, the motor develops self-sustained oscillations that reach a limit cycle at a well defined frequency with a large oscillation amplitude, characterized in Figure 2 by a high root-mean-square (RMS) value of the pressure signal at the motor head-end.

DOI: 10.13009/EUCASS2017-64



Finally, the volumetric heat release rate $\dot{q}$ associated with the combustion of $N_p$ aluminum droplets per unit volume combustion is given by :

$$\dot{q} = N_p \dot{m} \Delta h_r \tag{7}$$

One important feature of this combustion model is that the combustion reaction ceases, *i.e.* $\dot{m}$ is set to zero in the simulation, when the aluminum droplet diameter $D$ drops below the alumina residue diameter $D_{res}$.

## 3. Numerical model

The results presented in this work are obtained by numerical simulations with the CPS in-house Airbus Safran Launcher flow solver[24] and the aluminum droplet combustion model presented in the previous section.

This code solves the compressible Navier-Stokes equations with a finite volume technique over unstructured meshes. It assumes a perfect gas law for the gaseous phase. A two-way coupling Eulerian model is used to model the two-phase flow dynamics. The dense phase is assumed to be enough diluted with a monodisperse distribution of spherical droplets. Conservative variables are computed at the center of the cells of the numerical domain, whereas convective fluxes are computed at cell edges using an approximate Roe-Riemann numerical scheme for the gaseous phase and a Roe-Donor scheme for the particle phase. The simulations presented in this work are second order accurate in space with a MUSCL approach and forth order accurate in time using an explicit four steps Runge-Kutta time stepping. The time step is given by a Courant-Friedrichs-Lewy condition set to $CFL = 0.55$. All computations are carried out in a 2D axisymmetric formulation.

The geometrical configuration investigated is shown in Figure 3 and corresponds to a cylindrical motor with a radial injection of mass modeling the solid propellant combustion and a nozzle. This simplified model features the main elements of a large SRM. The chamber radius is $R = 0.593$ m and its length is $L = 7$ m. The nozzle has a throat of radius $R_t = 0.175$ m, which is located at $x_t = 7.3$ m away from the motor head-end. Only one half of the motor is computed and shown in Figure 3 due to rotational symmetry of the motor in the azimuthal direction.

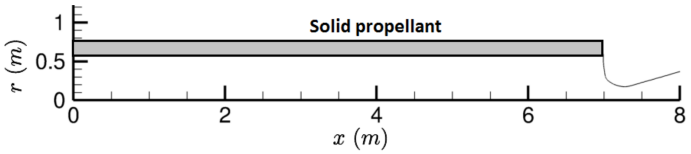


Figure 3: SRM geometry used for the simulations.

The computational grid is composed of 170,000 quads with about 600 points in the axial direction and 280 points in the radial direction. The grid is clustered near the propellant burning surface to resolve the aluminum distributed combustion where the thermo-acoustic coupling takes place. A posteriori analysis of computations shows that about 70 grid points lie in the combustion zone of aluminum particles. The smallest grid spacing at the propellant surface is about 1 mm. Grid convergence has been checked by running simulations on a 440,000 grid points mesh and no significant differences have been noted for the pressure, velocity and heat release rate fields recorded at different locations in the motor. Gas and aluminum particle properties are compiled in Table 1. These data are typical of aluminum particle combustion in SRM.[7,8]

Table 1: Gas and particle properties in a SRM[8]

| $\mu$ [kg/m/s] | Sc [-] | $\gamma$ [-] | $C_{P,p}$ [J/kg/K] | $C_{P,g}$ [J/kg/K] | $\rho_{Al}$ [kg/m$^3$] | $\Delta h_{r,0}$ [J/kg] | $L_v$ [J/kg] | $T_{sat}$ [K] |
|---|---|---|---|---|---|---|---|---|
| $9.1 \times 10^{-5}$ | 0.4 | 1.16 | 1177 | 2000 | 2000 | $9.53 \times 10^6$ | $10.8 \times 10^6$ | 2791 |

The density of aluminum droplets or alumina residue $\rho_{Al}$ is taken constant. During the combustion process, the particle temperature is supposed to be constant and equal to the saturation temperature $T_{sat}$. The droplets are injected in the numerical domain at this temperature $T_{p,i} = T_{sat}$. It is worth noting that turbulence is not taken into account in the simulations presented in this work. This is admittedly a rough approximation of reality, but allows to focus the analysis on the coupling between acoustics and aluminum particle unsteady combustion without taking into account the complex interactions with the turbulent flow field.

No-slip conditions are used for the gaseous phase at the wall boundaries including the head-end and the nozzle. The centerline $r = 0$ is a symmetry axis. Solid propellant burning is modeled through the lateral boundary condition of the numerical domain between $x = 0$ and $L = 7$ m by injection of gas at a constant mass flow rate with a velocity

DOI: 10.13009/EUCASS2017-64



vector normal to the surface and pointing inward. The propellant burnt gases are injected in the numerical domain at $T_{g,i}$ and the aluminum particles at $T_{p,i}$.

Results from Fabignon et al.[25] are used to determine droplet injection conditions. For a solid propellant loaded with 18% aluminum in mass, one-third of this aluminum agglomerate. Two classes of injected droplet can be distinguished: agglomerated droplets and non-agglomerated droplets. The non-agglomerated droplets are the smallest and burn faster and close to the solid propellant injection, where the velocity fluctuations could be neglected. To facilitate our analysis of the thermo-acoustic coupling, we consider only the agglomerated particles, modeled by a single class of droplets. So, only one third of the aluminum fraction is injected in our computation, corresponding to $Y_{Al,i} = 0.06$ (for a 18% Al propellant) at an initial diameter $D_i = 120\ \mu$m. For the reference simulation, the alumina residue diameter is fixed to $D_{res} = 60\ \mu$m. Aluminum particles are injected with a diameter $D_i = 120\ \mu$m at the same velocity as the gas $\mathbf{u_{p,i}} = \mathbf{u_i}$ and the injected gas-particle mass flow rate due to the solid propellant combustion is $\rho_i|\mathbf{u}_i| = 24.63$ kg/m$^2$/s. Boundary conditions and combustion model parameters are summarized in Table 2.

Table 2: Injection boundary conditions and combustion model parameters for the reference simulation.

| $\rho_i\|\mathbf{u}_i\|$ [kg/m$^2$/s] | $T_{g,i}$ [K] | $Y_{Al,i}$ [-] | $T_{p,i}$ [K] | $D_i$ [$\mu$m] | $D_{res}$ [$\mu$m] |
|---|---|---|---|---|---|
| 24.63 | 3450 | 0.06 | 2791 | 120 | 60 |

## 4. Analysis of the reference configuration

It is recalled that simulations of the reference case are made for a laminar flow and uniform mass injection through the propellant boundary. The propellant combustion response to pressure disturbances is not taken into account in these simulations.

### 4.1 Analysis of pressure signals

As already observed by Gallier and Godfroy[8] in a very similar configuration, a thermo-acoustic instability takes place around the first acoustic axial mode 1L of the motor and reaches a stable limit cycle. Figure 4 shows the pressure signal at limit cycle of the instability at the head-end location ($x = 0$). The oscillation frequency of this signal is $f \approx 70.5$ Hz, a value close to the pure acoustic mode frequency $f_a \approx 76$ Hz of the motor. The average pressure is around $p_0 = 10.383$ MPa and the amplitude of the pressure fluctuations is $\eta = 10.5$ kPa.

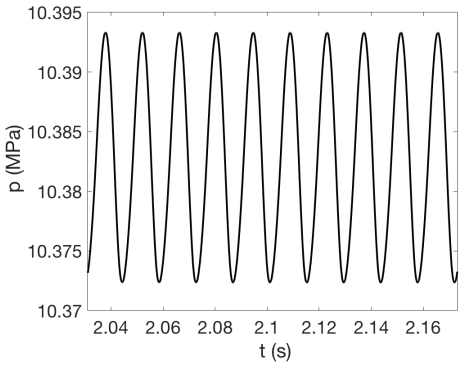


Figure 4: Head-end pressure history recorded for the reference simulation.

Another interesting quantity to calculate is the growth rate $\alpha_c$ of the thermo-acoustic instability given by:[1]

$$\alpha_c = \frac{1}{T}\int_T \frac{\gamma - 1}{\gamma p_0 E^2}\int_V p'\dot{q}' dV dt \tag{8}$$

where $p'$ and $\dot{q}'$ are the local pressure and volumetric heat release rate fluctuations, $\gamma$ is the ratio of heat capacities and $E$ denotes the acoustic energy in the motor volume $V$:

$$E^2 = \int_V \left(\frac{\rho_0 u'^2}{2} + \frac{p'^2}{2\rho_0 c_0^2}\right) dV \tag{9}$$

DOI: 10.13009/EUCASS2017-64



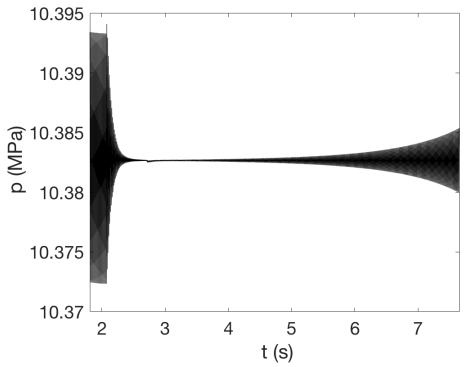


Figure 5: Pressure signals used to determine the growth rate of the thermo-acoustic instability.

In this expression, $\rho_0$ is the mean density and $c_0 = (\gamma p_0/\rho_0)^{1/2}$ the speed of sound.

The growth rate $\alpha_c$ cannot directly be determined from the numerical simulation due to acoustic losses through the SRM nozzle, attenuation by the solid propellant combustion and from the residue droplets.[8] Let associate these losses to a decay rate $\alpha_l < 0$ of the acoustic pressure inside the motor. The following method is used to determine these growth rates. It is described here for the reference case but is also used for the other unstable cases investigated.

Simulations are first carried out to let the pressure signal reach a limit cycle as in Figure 4. The fluctuations $\dot{m}'$ of the mass consumption rate $\dot{m}$ of aluminum particles are then abruptly set to zero in the simulations. By doing so, the thermo-acoustic source is removed and the acoustic pressure decreases in the system due to acoustic losses as shown in Figure 5 between instants 2.2 s $\leq t \leq$ 2.8 s. This test also confirms that the instability observed in the simulation is due to the coupling between unsteady combustion of aluminum particles and acoustics. As the pressure fluctuations decrease in the system and are about to vanish, the envelope of the pressure signal takes the form of an exponential decay $\sim \exp(-\alpha_l t)$ from which $\alpha_l$ is deduced.

When pressure oscillations have disappeared, thermo-acoustic coupling is reactivated in the simulation by allowing fluctuations of the mass burning rate of aluminum droplets. This is made at time $t > 2.9$ s in Figure 5 and pressure oscillations start again to increase exponentially with a growth rate $\alpha = \alpha_l + \alpha_c$. This quantity is again deduced from the envelope of the oscillations shown in Figure 5 before the emergence of nonlinear effects that saturate the signal to a limit cycle. The difference between the two measured growth rates yields the growth rate $\alpha_c$ associated to the thermo-acoustic source.

For the reference conditions one finds $\alpha_l = -14$ s$^{-1}$ and $\alpha_c = 15$ s$^{-1}$.

### 4.2 Analysis of heat release rate signals

Figure 6 shows the mean volumetric heat release rate distribution $\dot{q}_0$ in the motor due to aluminum particle combustion integrated over an oscillation period $T = 1/f$ when the system has reached the limit cycle shown in Figure 4 :

$$\dot{q}_0 = \frac{1}{T}\int_T \dot{q}dt \tag{10}$$

Figure 6 is a zoom over the combustion zone that has been stretched in the radial direction $r$. This figure shows that the combustion of aluminum droplets takes place very close to the solid propellant surface and the thickness of the combustion region changes along the longitudinal direction. Combustion of aluminum droplets takes essentially place in the boundary layer of the flow along the propellant surface over a radial distance less than 2.3 cm that can be compared to the radius $R = 59.3$ cm of the motor chamber. The heat release distribution is also found to be non-uniform with an increasing energy release in the axial direction.

The heat release distribution is now analyzed at limit cycle during an oscillation period $T = 1/f$ in Figure 7. The level of heat release is fluctuating inside the combustion volume in the longitudinal direction. This oscillation of the distribution of the heat release rate is already known to constitute a powerful thermo-acoustic source which either damp or amplify pressure disturbances depending on their phase relationship with respect to heat release.[8]

One also clearly identifies in Figure 7 a large motion of the boundary where heat release rate fluctuations take place. The displacement of the combustion zone in the acoustic field has been shown to be the source of thermo-acoustic instabilities coupled to high-frequency transverse modes in liquid rocket motors.[26–29] The motion of the boundary of the combustion zone of aluminum droplets has however so far not been reported in previous works on SRM combustion

DOI: 10.13009/EUCASS2017-64



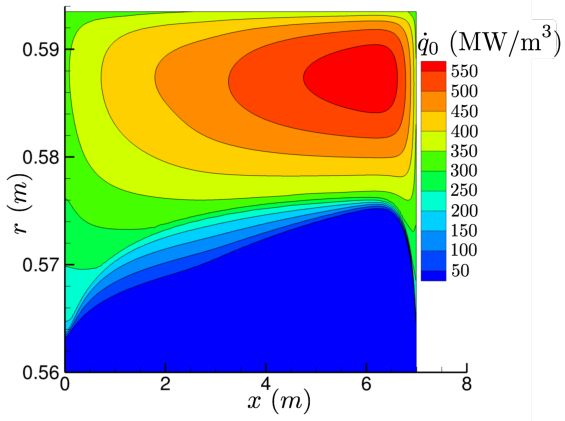


Figure 6: Mean volumetric heat release rate distribution $\dot{q}_0$ from aluminum particle combustion. Zoom over the combustion region.

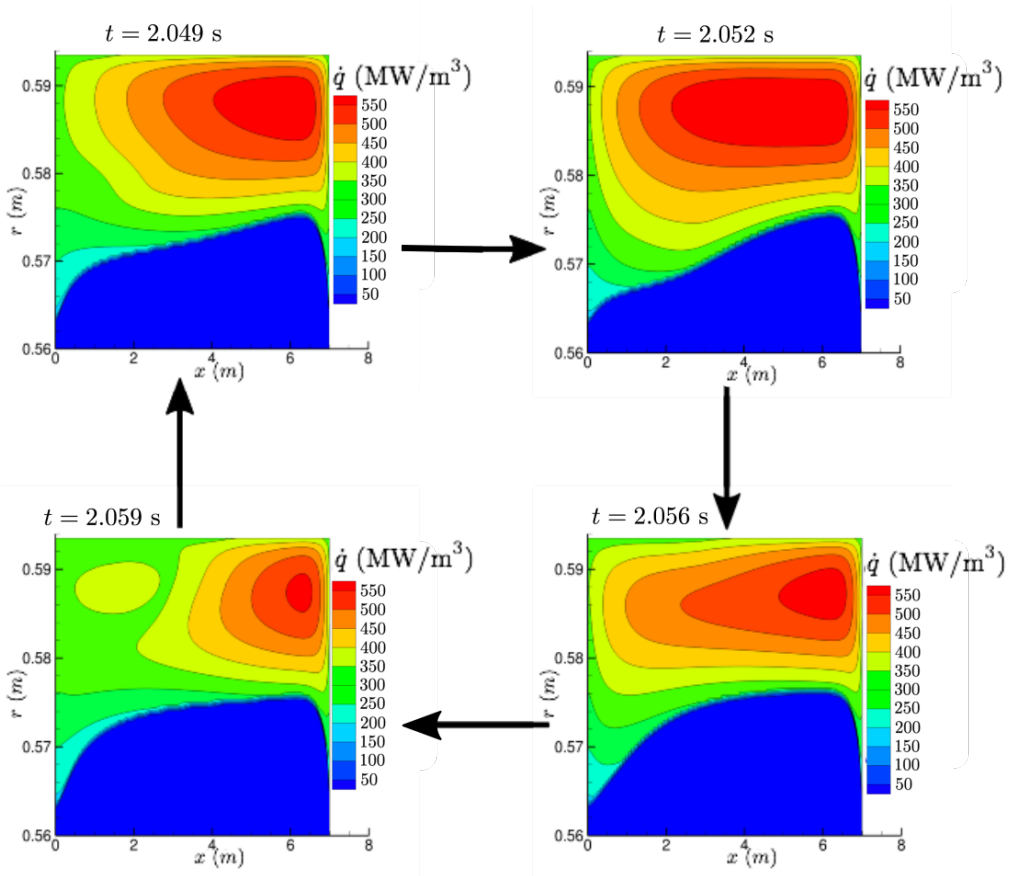


Figure 7: Volumetric heat release rate distribution at different instants during one oscillation period at the instability limit cycle. ($T = 1/f = 0.0142$ s)

instabilities. It constitutes an additional source of destabilization of the motor that needs to be considered. This motion has also so far been neglected in analytical acoustic energy balance analysis of aluminum particle combustion driven thermo-acoustic instabilities.[8]

DOI: 10.13009/EUCASS2017-64



### 4.3 Contributions to heat release fluctuations

The heat release response $\dot{q}'$ of an isolated droplet submitted to an oscillating flow has been investigated theoretically and numerically.[8,30] Assuming that disturbances of aluminum particle density $N_p$ and enthalpy reaction $\Delta h_r$ can be neglected, heat release rate fluctuations $\dot{q}'$ are due to oscillations of the aluminum droplet burning rate $\dot{m}'$ of each droplet :

$$\dot{q}' \simeq N_p \Delta h_r \dot{m}' \tag{11}$$

Assuming harmonic disturbances, one may write each fluctuating quantity as $a' = \mathcal{R}[\hat{a}\exp(-i\omega t)]$, where $\hat{a}$ denotes the Fourier component of the signal $a'$ associated to the angular pulsation $\omega$ and the operator $\mathcal{R}[\cdot]$ takes the real component of the complex expression in brackets.

Disturbances of the burning rate $\dot{m}'$ are associated to longitudinal and radial velocity, temperature and density fluctuations. Numerically, it is found that the response to temperature, density and radial velocity fluctuations can be neglected. Only the response to the longitudinal velocity disturbances is therefore taken into account here. However, diameter responses to velocity fluctuations have been neglected. Under these assumptions, heat release fluctuations $\dot{q}'$ are given in the Fourier space by :

$$\hat{\dot{q}} = \mathcal{H}_{u,0} \frac{\dot{q}_0}{|\delta \mathbf{u}_{\mathbf{p},\mathbf{0}}|^2 / \delta u_{p,0}} \hat{u} \tag{12}$$

where the mean quantities are calculated as $\delta \mathbf{u}_{\mathbf{p},\mathbf{0}} = \frac{1}{T}\int_T \delta \mathbf{u}_\mathbf{p} dt$, $\delta u_{p,0} = \frac{1}{T}\int_T \delta u_p dt$ which is the difference between the mean particle and gas velocities projected on the $x$-axis, $\dot{q}_0 = \frac{1}{T}\int_T \dot{q} dt$ and $\mathcal{H}_{u,0} = \frac{1}{T}\int_T \mathcal{H}_u dt$. The transfer function $\mathcal{H}_{u,0}$ is given by:[8,30]

$$\mathcal{H}_u = \frac{\mathrm{Sh} - 2}{2\mathrm{Sh}} \frac{\omega\tau_v(i - \omega\tau_v)}{1 + \omega^2\tau_v^2} \tag{13}$$

where $\omega = 2\pi f$ is the angular pulsation and $\tau_v$ is the inertial characteristic time, which is calculated by the Clift correlation[31] and given by:[8]

$$\tau_v = \frac{1 + B}{1 + 0.15\mathrm{Re}_p^{0.687}} \frac{\rho_{Al} D^2}{18\mu} \tag{14}$$

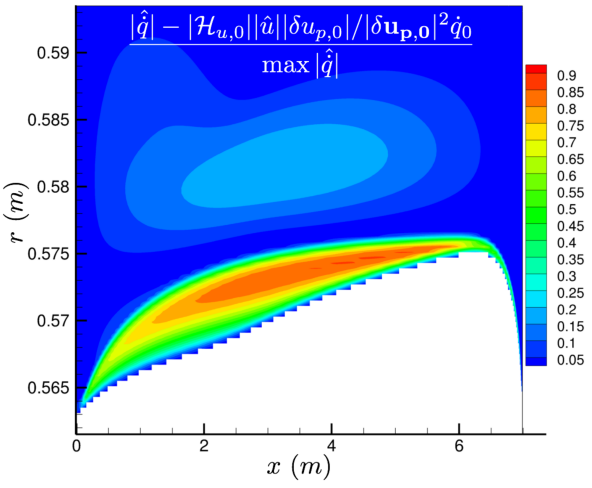


Figure 8: Difference between heat release rate fluctuations calculated with Eq. (12) and values extracted from the simulation.

The different terms of Eq. (12) are determined in this work using the numerical data at the limit cycle. The mean and fluctuating quantities can easily be extracted since the oscillations are almost harmonic (see Figure 4). The quantities $\mathcal{H}_{u,0}$, $\dot{q}_0$, $|\hat{\dot{q}}|$, $|\hat{u}|$ are calculated by post-processing the numerical data. According to Eq. (12) one has the following equality :

$$|\hat{\dot{q}}| = |\mathcal{H}_{u,0}| \frac{\dot{q}_0}{|\delta \mathbf{u}_{\mathbf{p},\mathbf{0}}|^2 / |\delta u_{p,0}|} |\hat{u}| \tag{15}$$

DOI: 10.13009/EUCASS2017-64



Figure 8 shows the difference between the modulus of the Fourier component associated to the volumetric heat release rate fluctuation $|\hat{\dot{q}}|$ extracted from the simulation and the prediction from Eq. (15). These quantities are all computed at limit cycle. The difference between these terms is non-negligible ($\sim 10-20\%$) within the combustion volume, indicating that in the Eq. (12) is not totally correct. In fact, the diameter of the droplets respond to the velocity fluctuations and they are not modeled in the Eq. (12). Moreover, this difference rapidly increases at the free boundary of the combustion zone ($\sim 60-80\%$) where oscillations of this surface have been highlighted in Figure 7. The motion of the aluminum combustion boundary is not taken into account in the analytic model Eq. (12) and constitutes an additional thermo-acoustic source.[27]

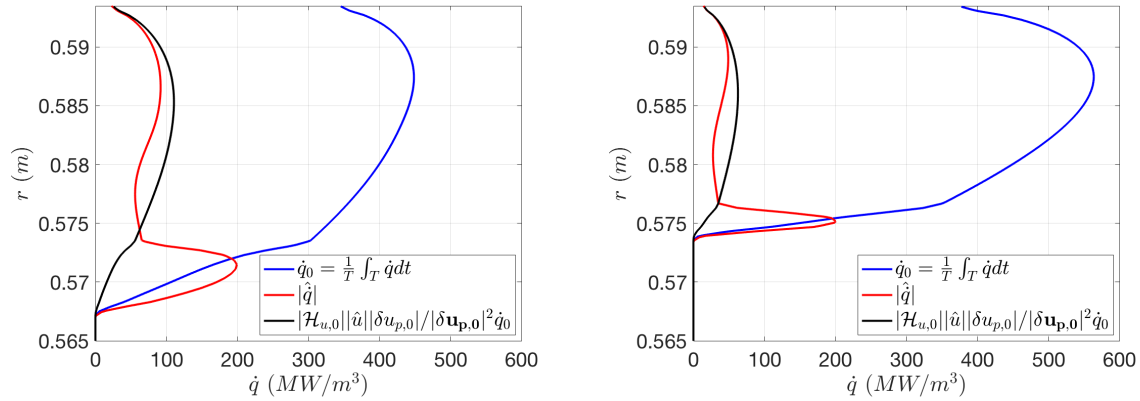


(a) $x/L = 1/4$ (b) $x/L = 3/4$

Figure 9: Radial distributions of the volumetric mean heat release rate $\dot{q}_0$, the modulus of its fluctuation $|\hat{\dot{q}}|$ and prediction deduced from Eq. (12) at two positions in the SRM.

These observations are confirmed in Figure 9, where predictions from Eq. (12) and the numerical results are compared at two axial positions $x/L = 1/4$ and $x/L = 3/4$ in the chamber. The mean heat release distribution is also plotted in this figure. At $x/L = 1/4$, aluminum droplet combustion takes place over a slightly larger distance to the propellant surface than at $x/L = 3/4$, but the volumetric energy release is a bit higher at $x/L = 3/4$ compared to the values found at $x/L = 1/4$. The black curves show predictions from Eq. (12) which could be a good approximation of the red curves plotting $|\hat{\dot{q}}|$ extracted from the simulations, except near the lower boundary of the combustion zone. In this region, the mean heat release shown in blue in Figure 9 rapidly decreases with a steep radial gradient and the fluctuations $|\hat{\dot{q}}|$ plotted in red are of the same order as the mean values. These heat release oscillations associated to the flapping motion of the combustion boundary are not reproduced by the analytic model Eq. (12) and the difference in the combustion volume is certainly due to the non-modeled diameter fluctuations. These two contributions of the heat release rate fluctuations are designated, respectively, as the boundary contribution (B.C.) and the volumetric contribution (V.C.).

An integration of the heat release rate oscillation along the radial direction indicates that the motion of the boundary (B.C.) contributes to 37% to the total heat release rate fluctuation in the motor slice at $x/L = 1/4$ and to 36% at $x/L = 3/4$. The model Eq. (12) taking into account the response of an isolated droplet to an oscillating flow thus only reproduces, partially, about 60% (V.C.) of the total heat release fluctuation $\int_V |\hat{\dot{q}}|dV$ within the motor. The mechanism associated to the motion of the boundary of the combustion volume is missing in this analysis.

This boundary is defined in the simulation by the condition $D = D_{res}$. Combustion ceases when the aluminum droplet diameter $D$ falls below the critical value $D_{res}$ of the aluminum residue. The motion of this boundary indicates that the burning rate of an aluminum droplet is altered by the acoustic field when a combustion droplet is about to extinguish. Fluctuations of the burning rate due to the oscillating flow take indeed place all along the trajectory of the aluminum droplets and obey to Eq. (11). For each individual droplet, oscillations of their burning rate lead to fluctuations of their diameter that regularly decreases in average as combustion proceeds with an oscillating pattern. The lifetime of each aluminum droplet, *i.e.* the combustion time, is thus also altered by the acoustic oscillation and depends on the history of the aluminum particle along its trajectory within the oscillating flow. In other words, the diameter fluctuations are the cause of the boundary motion verifying the condition $D = D_{res}$ and of the difference between the model Eq. (12) and the numerical result in the combustion volume.

To consider these droplet diameter fluctuations, it is necessary to take in account the local diameter fluctuations and an history effect in the linear model Eq. (12). In the current model,[8,30] volumetric heat release rate disturbances $\dot{q}'$ do not take into account the history of the diameter fluctuations experienced by the droplet from its release to the

DOI: 10.13009/EUCASS2017-64



local state. This model cannot thus reproduce the motion of the boundary of the end combustion of aluminum droplets, which is the consequence of each droplet mass burning rate history.

A parametric study is conducted in the next section by varying the aluminum mass consumption rate at the end of the combustion process to emphasize the contribution of the motion of the boundary of the aluminum droplet combustion volume to the total heat release oscillation in the SRM and to the thermo-acoustic instability.

## 5. Effects of the combustion model

It has been shown that there are two contributions to heat release fluctuations in a SRM originating from fluctuations within the combustion volume occupied by the aluminum particles and from the motion of the boundary of this volume. This motion depends on the history of the burning rate along the aluminum droplet trajectories before combustion ceases when the particle diameter drops below $D_{res}$. The residue diameter which is a parameter of the combustion model defines when and where the aluminum combustion ceases.

Simulations are now conducted by varying the residue diameter $D_{res}$ from 50 to 70 $\mu$m in the combustion model to further investigate effects of the end-life of aluminum particles on combustion instabilities. For the same mass of aluminum injected in the SRM and for the same aluminum droplet injection diameter $D_i = 120\,\mu$m, the thermodynamic equilibrium in the chamber changes when the particle residue diameter is modified. If the residue diameter is bigger than the reference residue diameter, less energy is released by the aluminum combustion and the mass fraction of residue is higher. To keep the same particle-gaz thermodynamic equilibrium, injection conditions are thus slightly modified as indicated in Table 3.

Table 3: Injection conditions for the parametric analysis.

| $D_{res}$ [$\mu$m] | 50 | 60 | 70 |
|---|---|---|---|
| $T_{g,i}$ [K] | 3438 | 3450 | 3466 |
| $C_{P,g}$ [J/kg/K] | 1997 | 2000 | 2004 |
| $\gamma$ [-] | 1.1597 | 1.1600 | 1.1605 |

Figure 10 shows an example of the evolution of the mean burning rate $\dot{m}_0$ of a single aluminum particle as a function of time when $D_{res}$ is modified and the Sherwood number is equal to $Sh = 2$ (no convection effect). The residue diameter fixes the aluminum mass consumption rate value at the end of the droplet combustion, the combustion time and the combustion thickness (combustion volume).

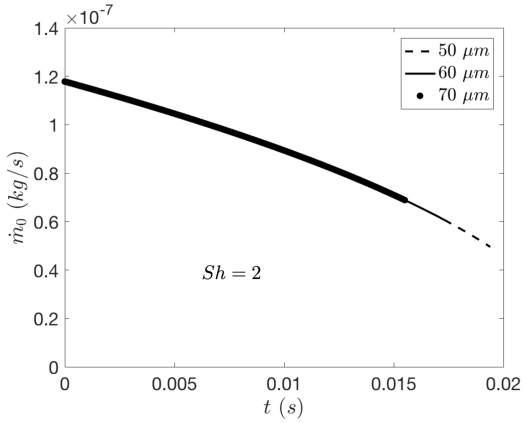


Figure 10: Impact of the residue diameter $D_{res}$ on the mean aluminum droplet burning rate $\dot{m}_0$ at $Sh = 2$. Particles are injected with a diameter $D_i = 120\,\mu$m and at injection conditions synthesized in Table 3.

Figure 11 shows results for the grow rates of the pressure signal and at limit cycle at the head-end of the SRM. The growth rates $\alpha_c$ and $\alpha_l$ are determined with the methodology described in section 4.1. The oscillation amplitude $\eta$ and frequency $f$ are determined at the instability limit cycle. One reminds that simulations for $D_{res} = 60\,\mu m$ lead to a thermo-acoustic instability with a positive growth-rate $\alpha_c + \alpha_l = 1\ s^{-1}$ that reaches a limit cycle with a pressure oscillation amplitude of $\eta = 10.5$ kPa at a frequency $f = 70.5$ Hz locked on the first acoustic axial mode 1L of the motor.

DOI: 10.13009/EUCASS2017-64



When the residue diameter is increased to $D_{res} = 70\ \mu$m, the system is also found to be unstable with heat release induced pressure disturbances characterized by a growth rate $\alpha_c = 20.8\ s^{-1}$ exceeding the damping rate $\alpha_l = -14.8\ s^{-1}$ of acoustic losses in the SRM. Pressures oscillations reach in this case a limit cycle at a frequency $f = 71.8$ Hz with an amplitude of $\eta = 13.7$ kPa. The difference between this configuration and the reference case is mainly due to changes of the thermo-acoustic source between simulations conducted at $D_{res} = 60\ \mu$m and $70\ \mu$m where $\alpha_c = 15.0\ s^{-1}$ and $20.8\ s^{-1}$ respectively, while acoustic damping is less altered and only changes from $\alpha_l = -14.0\ s^{-1}$ to $-14.8\ s^{-1}$ respectively.

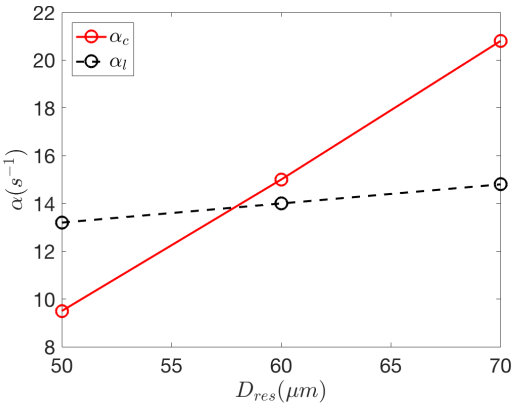


| $D_{res}$ | [$\mu$m] | 70 | 60 | 50 |
|---|---|---|---|---|
| $\alpha_c$ | [1/s] | 20.8 | 15.0 | 9.5 |
| $\alpha_l$ | [1/s] | -14.8 | -14.0 | -13.2 |
| $\alpha_c + \alpha_l$ | [1/s] | 6.0 | 1.0 | -3.7 |
| $\eta$ | [kPa] | 13.7 | 10.5 | – |
| $f$ | [Hz] | 71.8 | 70.5 | – |

Figure 11: Left : Pressure signal growth rates $\alpha_c$ and $\alpha_l$ as a function of the alumina residue diameter $D_{res}$. Right : synthesis of results for an instability characterized by the growth rates $\alpha_c$ and $\alpha_l$ and at instability limit cycle of amplitude $\eta$ and frequency $f$.

When the residue diameter is reduced to $D_{res} = 50\ \mu m$ compared to the reference case, the SRM is now found to be thermo-acoustically stable. The growth rate of pressure disturbances are determined in this case by submitting the SRM to an external small harmonic pressure oscillation at the frequency of the reference computation limit cycle $f = 70.5$ Hz until the system reaches a stable oscillation and then the forcing is stopped. At this stage, the pressure oscillation amplitude at the head-end of the SRM begins to decrease from which a (negative) growth rate $\alpha = \alpha_c + \alpha_l = -3.7\ s^{-1}$ is deduced and reported in Figure 11. By extrapolating the acoustic losses from the values found at the two other residue diameters, one finds $\alpha_l = -13.2\ s^{-1}$ and deduces that the thermo-acoustic coupling yields in this case a growth rate $\alpha_c = 9.5\ s^{-1}$.

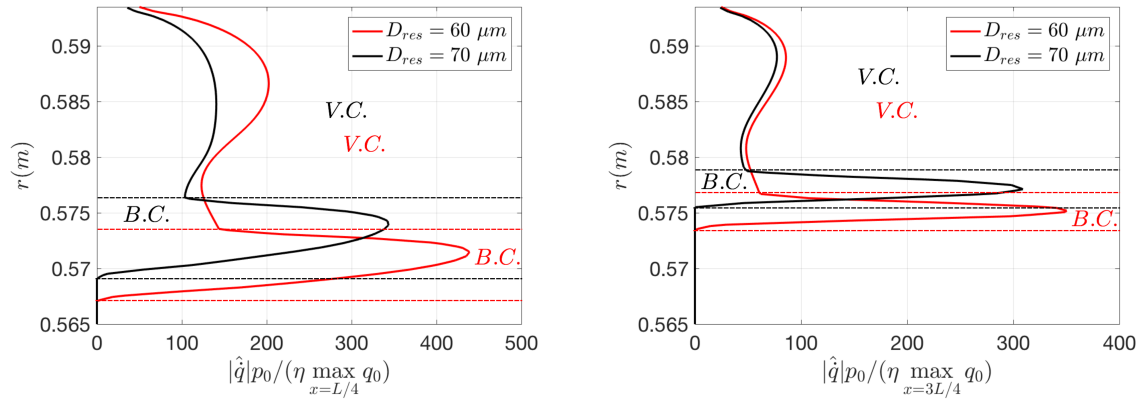


(a) $x/L = 1/4$ (b) $x/L = 3/4$

Figure 12: Normalized heat release fluctuation modulus for $D_{res} = 60\ \mu m$ and $D_{res} = 70\ \mu m$ at $x/L = 1/4$ (a) and $x/L = 3/4$ (b). V.C. : volumetric contribution. B.C. : boundary contribution.

The main conclusion from this parametric analysis, is that the thermo-acoustic instability source strength increases more rapidly with the alumina residue diameter $D_{res}$ than the acoustic losses as shown on the left in Figure 11. In other words, changes of the residue diameter have more consequences on the thermo-acoustic source than on the acoustic losses.

DOI: 10.13009/EUCASS2017-64



Table 4: Heat release fluctuation radial distribution at $x/L = 1/4$ and $3/4$ as a function of the alumina residue diameter.

| | $x/L = 1/4$ | | $x/L = 3/4$ | |
|---|---|---|---|---|
| $D_{res}$ [$\mu$m] | B.C. | V.C. | B.C. | V.C. |
| 70 | 44% | 56% | 41% | 59% |
| 60 | 37% | 63% | 36% | 64% |

The aluminum mass consumption rate and thus the heat release rate at the end of the droplet combustion highly depends on the residue diameter as shown in Figure 10. To better understand this behavior, Figure 12 shows the normalized distributions of heat release rate fluctuations at the instability limit cycle oscillation frequency $f$ for the simulations conducted with $D_{res} = 60$ and 70 $\mu$m. Results are again presented at two positions $x/L = 1/4$ and $x/L = 3/4$ in the SRM. These graphs indicate that increasing the residue diameter $D_{res}$ leads to a reduction of the extension of the combustion volume in the radial direction due to a shorter combustion time. The distributions of heat release fluctuations can be separated in two zones in Figure 12. The first one designated as V.C. for volumetric contribution is the closest to the propellant surface. The inflection point of the heat release fluctuation defines the end of the V.C. zone and the beginning of the B.C. zone, which stands for boundary contribution to heat release fluctuations near the end of the aluminum combustion zone. One clearly see that changing the residue diameter $D_{res}$ both affect the distribution of heat release fluctuations in the V.C. and B.C. zones.

Table 4 indicates after integration over a radial slice through the motor the heat release fluctuation distribution between the V.C. and B.C. zones. The distribution of heat release disturbances between the V.C. and B.C. zones depends on the residue diameter and the boundary contribution represent about a bigger significant percentage of the total fluctuation for a bigger residue diameter than the reference computation.

## 6. Conclusion

Aluminum particle combustion driven thermo-acoustic instabilities in SRM have been investigated in a generic configuration with a fully compressible Navier Stokes solver and a two-phase model for aluminum droplet combustion and transport. It has been found that the origin of unsteady heat release disturbances leading to self-sustained synchronized pressure oscillations in the motor is due to oscillations of the burning rate of each aluminum droplet within the acoustic field of the motor and to a motion of the boundary where aluminum droplet combustion takes place.

Simulations carried out at limit cycles of instabilities reveal that heat release oscillations take place close to the solid propellant surface in the acoustic boundary layer of the flow. Contributions to heat release disturbances in the SRM may be split in fluctuations associated to changes of the aluminum droplet burning rate within a fixed combustion volume and to changes of the boundary of this combustion volume. The volume contribution (V.C.) model could be improved, considering the diameter fluctuations. The boundary contribution (B.C.) has so far been neglected in many thermo-acoustic models of SRM and may represent up to 40% of the total unsteady heat release rate in the simulations conducted in this work. The contributions to the total heat release oscillation in the motor associated with changes within the volume and at the combustion volume boundary are sensitive to the alumina residue diameter. The growth rate of heat released induced pressure disturbances is shown to linearly increase with the residue diameter of the alumina particles and is also found to be related to the motion of the combustion volume boundary.

The motion of the boundary of the combustion zone defined by the condition $D = D_{res}$ in the simulations, where $D_{res}$ designates the diameter of the alumina residues of aluminum droplets, is believed to be the consequence of the fluctuations of the aluminum droplet diameter along their trajectory through the motor. These diameter fluctuations are the consequence of the history of the burning rate oscillations along the droplet life and the consequence of the boundary motion. This indicates in turn that oscillations of the burning rate due to acoustic coupling lead to changes of the aluminum droplet diameters and this contribution needs to be taken into account in theoretical models to reproduce the correct level and distribution of the heat release rate at the end of the combustion volume in the SRM.

DOI: 10.13009/EUCASS2017-64



## 7. Acknowledgments

This work was part of an ongoing PhD thesis which is cofunded by the French space agency Centre National d'Etudes Spatiales (CNES) and Airbus Safan Launchers (ASL).

## References

[1] F. E. C. Culick and P. Kuentzmann. Unsteady motions in combustion chambers for propulsion systems. Technical report, DTIC Document, 2006.

[2] F. E. C. Culick and V. Yang. Prediction of the stability of unsteady motions in solid-propellant rocket motors. 1992.

[3] F. Vuillot and N. Lupoglazoff. Combustion and turbulent flow effects in 2-D unsteady navier-stokes simulations of oscillatory rocket motors. *Proceedings AIAA 96*, 884:15–18, 1996.

[4] S. Gallier, J.F. Guery, F. Godfroy, P. Le Breton, D. Ribereau, and P. Cloutet. Instabilités de fonctionnement dans les moteurs à propergol solide de grande taille. *Revue Scientifique et Technique de la Défense (57)*, page 17, 2002.

[5] Y. Fabignon, J. Dupays, G. Avalon, F. Vuillot, N. Lupoglazoff, G. Casalis, and M. Prévost. Instabilities and pressure oscillations in solid rocket motors. *Aerospace science and technology*, 7(3):191–200, 2003.

[6] K. P. Brooks and M. W. Beckstead. Dynamics of aluminum combustion. *Journal of Propulsion and Power*, 11(4):769–780, 1995.

[7] J. Dupays and F. Vuillot. Propagation of an acoustic wave in a two-phase reactive medium. In *34th AIAA/ASME/SAE/ASEE Joint Propulsion Conference and Exhibit*, page 3696, 1998.

[8] S. Gallier and F. Godfroy. Aluminum combustion driven instabilities in solid rocket motors. *Journal of propulsion and power*, 25(2):509–521, 2009.

[9] M. W Beckstead and F. E. C. Culick. A comparison of analysis and experiment for solid propellant combustion instability. *AIAA Journal*, 9(1):147–154, 1971.

[10] J. Dupays and F. Vuillot. Propagation of acoustic waves in a two-phase vaporizing mixture. *Journal of propulsion and power*, 18(1):222–224, 2002.

[11] F. Blomshield. Historical perspective of combustion instability in motors-case studies. In *37th Joint Propulsion Conference and Exhibit*, page 3875, 2001.

[12] M. W. Beckstead. A summary of aluminum combustion. Technical report, NATO Document, 2004.

[13] C. K. Law. A simplified theoretical model for the vapor-phase combustion of metal particles. *Combustion Science and Technology*, 7(5):197–212, 1973.

[14] P. E. DesJardin, J. D Felske, and M. D. Carrara. Mechanistic model for aluminum particle ignition and combustion in air. *Journal of Propulsion and Power*, 21(3):478–485, 2005.

[15] R. L. Derr, H. B. Mathes, and J. E. Crump. Application of combustion instability research to solid propellant rocket motor problems. *AGARD Solid Rocket Motor Technol. 12 p(SEE N 80-10281 01-20)*, 1979.

[16] P. Bucher, R. A. Yetter, F. L. Dryer, T. P. Parr, D. M. Hanson-Parr, and E. P. Viceni. Flames structure measurement of single, isolated aluminum particles burning in air. In *Symposium (International) on Combustion*, volume 26, pages 1899–1908. Elsevier, 1996.

[17] R. Borghi and M. Champion. *Modélisation et théorie des flammes*. Editions Technip, 2000.

[18] D. B. Spalding. Combustion of fuel particles. *Fuel*, 30(1):121–130, 1951.

[19] W. A. Sirignano. *Fluid dynamics and transport of droplets and sprays*. Cambridge University Press, 1999.

[20] K. K. Kuo. *Principles of combustion*. 1986.

[21] C. K. Law. *Combustion physics*. Cambridge university press, 2006.

DOI: 10.13009/EUCASS2017-64



[22] W. E. Ranz and W. R. Marshall. Evaporation from drops. *Chemical Engineering Progress*, 48(3):141–146, 1952.

[23] M. W. Beckstead and K. P. Brooks. A model for distributed combustion in solid propellants. In *27th JANNAF Combustion Meeting, CPIA Publication*, volume 557, pages 237–258, 1990.

[24] P. Durand, B. Vieille, H. Lambare, P. Vuillermoz, G. Boure, P. Steinfeld, F. Godfroy, and J. Guery. CPS-A three dimensional CFD code devoted to space propulsive flows. In *36th AIAA/ASME/SAE/ASEE Joint Propulsion Conference and Exhibit*, page 3864, 2000.

[25] Y. Fabignon, J. F. Trubert, D. Lambert, O. Orlandi, and J. Dupays. Combustion of aluminum particles in solid rocket motors. In *39th AIAA/ASME/SAE/ASEE*, page 4807, 2003.

[26] Y. Méry. *Mécanismes d'instabilités de combustion haute-fréquence et application aux moteurs-fusées*. PhD thesis, Châtenay-Malabry, Ecole centrale de Paris, 2010.

[27] Y. Méry. Impact of heat release global fluctuations and flame motion on transverse acoustic wave stability. *Proceedings of the Combustion Institute*, 36(3):3889–3898, 2017.

[28] T. Hummel, F. Berger, M. Hertweck, B. Schuermans, and T. Sattelmayer. High-Frequency Thermoacoustic Modulation Mechanisms in Swirl-Stabilized Gas Turbine Combustors-Part II: Modeling and Analysis. *Journal of Engineering for Gas Turbines and Power*, 139(7):071502, 2017.

[29] F. M. Berger, T. Hummel, M. Hertweck, J. Kaufmann, B. Schuermans, and T. Sattelmayer. High-Frequency Thermoacoustic Modulation Mechanisms in Swirl-Stabilized Gas Turbine Combustors-Part I: Experimental Investigation of Local Flame Response. *Journal of Engineering for Gas Turbines and Power*, 139(7):071501, 2017.

[30] S. Gallier, F. Sibe, and O. Orlandi. Combustion response of an aluminum droplet burning in air. *Proceedings of the Combustion Institute*, 33(2):1949–1956, 2011.

[31] J. R. Grace, R. Clift, and M. E. Weber. Bubbles, drops and particles. *Academic Press, New York*, 1978.